Bayesian Paradigm to Assess Rock Compression Damage Models

Chloé Arson[1], Ph.D., School of Civil & Environmental Engineering, Georgia Institute of Technology, Atlanta, Georgia, USA

Zenon Medina-Cetina, Ph.D., Zachry Department of Civil Engineering, Texas A&M University, College Station, Texas, USA

---

1. Contact information:
Chloé Arson
School of Civil & Environmental Engineering
790 Atlantic Drive
Atlanta, GA 30332-0355
USA
Phone: (+1) 404-385-0143
E-mail: chloe.arson@ce.gatech.edu

Article type: paper (3000-5000 words with one illustration per 500 words).

Date text written or revised: first version submitted on 05/14/2013, first revision submitted on 07/31/2013, second revision submitted on 10/19/2013.

Number of words in the main text: 4,273.

Number of tables: 2.

Number of figures: 6 (with a total of 14 subfigures).

Abstract

Energy extraction and waste storage in geological formations raise interest in developing systematic and reliable calibration methods to assess rock models performance. A methodology is proposed to improve damage prediction in sandstone, based on Finite Element simulations coupled with the Bayesian paradigm. To illustrate this methodology, parameters of a Continuum Damage Mechanics model are defined as random variables. (1) First, probability density functions are formulated for each parameter (expert's judgement) and sampled later independently to simulate likely random sandstone responses during a triaxial compression test (forward problem). (2) Second, experimental data is introduced (new evidence available), which allows updating the probability distributions depicting the model parameters (inverse problem). Results show that it is possible to quantify the impact of experimental evidence into the rock characterization, and that correlations between all rock damage parameters can be retrieved. Mechanically speaking this means that: (a) similar accuracy in the prediction of damage might be achievable with less model parameters, (b) and the input of energy released to initiate crack propagation is contingent upon conditions external to the model (e.g., initial texture of the rock). Results from this investigation provide promising applications of the probabilistic calibration approach to damage models in multi-phase porous media.

Keywords chosen from *Environmental Geotechnics* list

010.1: Caprock; 016.8: Mechanical Geomaterial Characterization; 016.12: Tensile Strength; 022.5: Soil/Rock Mineral Alteration; 025: Numerical Methods; 029: Uncertainty, Reliability and Risk; 031.4: Radioactive Waste Disposals

List of notation

CDM	Continuum Damage Mechanics
REV	Representative Elementary Volume
PDF	Probability Density Function
RV	Random Variable
Ψ	rock solid matrix's Helmholtz free energy
$\boldsymbol{D}$	damage tensor
V_{DZ}	zone of influence of damage
Π_{frac}	potential energy of a fracture
A	surface area of a fracture
$\boldsymbol{n_k}$	normal direction of the k-th penny-shaped crack
d_k	volumetric fraction of the k-th penny-shaped crack
N	number of cracks in the REV
$\bar{E}(r,\mathbf{n})$	mathematical expectancy of the presence of a crack of radius r and normal direction $\boldsymbol{n}$
W_{ext}	work supplied by external forces to the REV
Π	potential energy stored in the REV
Q	heat transmitted to the REV
U_i	energy dissipated due to irreversible microstructure changes
$\boldsymbol{Y}$	energy release rate (to open cracks) / affinity
ε^E	elastic deformation tensor
ε^{el}	purely elastic deformation (in the absence of stiffness damage)
ε^{ed}	elastic deformation caused by stiffness damage
ε^{id}	irreversible damaged deformation
$\boldsymbol{C_{ref}}$	stiffness tensor of the virgin material (prior to loading)
$\boldsymbol{C(D)}$	damaged stiffness tensor
E	rock Young's modulus
g_M	resistance to crack closure
C_0	initial damage threshold
C_1	hardening parameter
$\boldsymbol{\theta}$	vector of (unknown, sought) parameters
$\boldsymbol{d_{obs}}$	vector of observed data
$\boldsymbol{\pi}(\boldsymbol{\theta})$	probability of $\boldsymbol{\theta}$ (prior)
$f(\mathbf{d}_{\mathbf{obs}}\|\boldsymbol{\theta})$	probability of $\boldsymbol{d_{obs}}$ knowing $\boldsymbol{\theta}$ (likelihood)
$\boldsymbol{\pi}(\boldsymbol{\theta}\|\mathbf{d}_{\mathbf{obs}})$	probability of $\boldsymbol{\theta}$ knowing $\boldsymbol{d_{obs}}$ (posterior)

1. Introduction

With the anticipated 50% increase in energy demand in the next 30 years, optimization of low-carbon emission fuel cycles has become a research priority for the twenty-first century. Spending less energy to build and maintain the infrastructure is one way to reduce emissions. This paper focuses on rock damage mechanics, which can be of interest for further research in geotechnical infrastructure reliability and performance assessment. Damage has to be defined relative to a reference state. Measures of damage depend on standards considered as relevant observation tools by the modeller. Prediction of damage is indirect (Arson & Gatmiri, 2008; Arson et al., 2012), and requires the selection of state and dissipation variables relevant to describe the anticipated "degradation" (e.g. deformation, stiffness, strength, wave velocity). Model formulation shall be dictated by principles and theories (e.g., thermodynamics, elasticity, micro-mechanics). Within a consistent theoretical framework, several formulations can be acceptable, and choosing the most relevant formulation may be impossible with a pure deterministic approach. In order to optimize mechanical damage formulation and calibration, it is proposed herein to combine principles of thermodynamics and the theory of Continuum Damage Mechanics (CDM) with the Bayesian paradigm (Medina-Cetina, 2006). The main characteristics and models of rock damage reported in the literature are summarized in Section 2. Section 3 presents a methodology to improve CDM predictions, based on Finite Element simulations coupled to Bayesian probabilistic analyses. To illustrate the concept of this methodology, four parameters of the rock damage model presented in (Arson and Gatmiri, 2010; 2012) were set as random variables. Results are presented in Section 4 where 7,000 parameters realizations were sampled in order to: (1) simulate likely responses of a sandstone subjected to a triaxial compression test, based on prior expert's judgement only, and (2) calibrate the damage parameters once experimental observations are made available.

2. Damage Characterization and Prediction in Rock

2.1. Rock Damage Characterization

In many energy geotechnical applications such as carbon dioxide sequestration (Xu et al., 2004), disposal of nuclear waste (Bonin, 1998; Gens et al., 1998; Blumling et al., 2007), storage of compressed air and natural gas (Cosenza et al., 1999; Slizowski and Walaszczyk, 2004), extraction of geothermal energy (Auqué et al., 2009), stress concentrations result from the displacement of the boundaries of a large discontinuity (typically: a cavity, a tunnel, a well bore, or a hydraulic fracture), which originates micro-cracks (Guéguen et al., 1996; Zimmermann et al., 2003). Underground laboratories are used to characterize rock mechanical, acoustic, and hydraulic properties in the Excavation Damaged Zone (e.g., Souley et al., 2001; Martino and Chandler, 2004; Tsang et al., 2005). Laboratory scale assessment of rock mechanical damage usually combine loading and unloading cycles with acoustic emissions, flow tests, porosimetry and/or imaging (e.g., Chan et al., 2001; Homand et al., 2002; Bera et al., 2011). Thermo-mechanical damage is usually assessed by performing temperature-controlled mechanical loading cycles, by conducting a heating phase followed by a mechanical loading, or by performing a heating phase followed by a relaxation period. Most of the published experimental results focus on rock compressive strength (see Zhu and Arson, 2014 for a literature review). Chemo-mechanical damage requires modeling frameworks that go beyond the framework of Continuum Damage Mechanics, because of the changes of pore shape and rock fabric induced by dissolution and precipitation (e.g. Raj, 1982; Spiers et al., 1990; Senseny et al., 1992).

2.2. Models of Transfer in Damaged Rock

Connections between cracks imply hydraulic crack interaction (i.e. enhanced permeability), but not necessarily mechanical crack interaction, especially if cracks are randomly oriented and if the distribution of cracks is dense (Schubnel et al., 2006). As a result, different damage variables have to be defined to capture different damage effects, such as permeability enhancement and stiffness degradation (Maleki and Pouya, 2010). Most of the damage models proposed for unsaturated porous media (such as rock and concrete) are based on Bishop's effective stress concept (Arson and Gatmiri, 2008). A damaged rigidity couples total stress to deformation, while the partial porosities are related to pore pressures through undamaged poro-elastic potentials. Damage thus remains uncoupled from fluid effects (Shao et al., 2005). Transfers in cracked porous media were extensively modelled with fracture network theories. The differences between such models lie in the number of represented continua and in the way fluid exchanges between media are taken into account (Durner, 1994; Vogel et al., 2000). Most fracture network models are restricted to the resolution of flow problems in a non-deformable matrix. Several models couple rock microstructure evolution to bulk partial porosities, which improves the prediction of permeability and retention properties in multi-modal porous networks (Garcia-Bengochea et al., 1979; Van Genuchten, 1980; Rieu and Sposito, 1991; Blunt, 2001; Romero and Jommi, 2008), including networks comprising natural pores and cracks (Arson,

2012; Arson and Pereira, 2013). Another approach consists in using tessellation techniques to measure the volume available for the flow from the knowledge of the surface area of the porous network, which can be computed by distinct element methods (Zangeneh et al., 2012).

2.3. Models of Rock Damage Mechanics

2.3.1. Micro-mechanical models

Micro-mechanical damage models (Pensée et al., 2002; Dormieux et al., 2006; Zhu et al., 2007; Levasseur et al., 2011) assume that rock Representative Elementary Volume (REV) is populated with a distribution of cracks characterized by a specific shape (usually, spherical, penny-shaped or ellipsoidal cracks). Assumptions on the shape and density of cracks allow expressing explicitly the strain concentration tensor, to further derive the theoretical expression of the Helmholtz free energy of the rock solid skeleton. For dilute distributions of cracks, the self-consistent method proved to provide an efficient scheme to model the loss of stored elastic deformation energy induced by cracking. If microscopic cracks open in pure mode I, i.e. if the crack displacement vector is parallel to the vector normal to the crack planes, the only damage variable needed to express the dissipation of energy associated to the degradation of elastic moduli is the second-order crack density tensor, defined by Kachanov (1992) as:

$$\mathbf{D} = \sum_{k=1}^{N} d_k \ \mathbf{n_k} \otimes \mathbf{n_k}$$

1.

In which the REV is assumed to contain N planar cracks with a normal direction $\boldsymbol{n_k}$ and a volumetric fraction d_k. Mixed crack propagation modes (inducing a non-zero tangential displacement at crack faces) require higher damage tensors – at least of order four (Chaboche, 1992; Halm and Dragon, 1998; Cauvin and Testa, 1999). Increasing the order of the damage tensor generally improves the compliance of the model to symmetry properties required for the elasticity tensor (Lubarda and Kracjinovic, 1993). In fact, the second-order density tensor emerging from micro-mechanical analyses is a particular form of Oda's fabric tensor, commonly used in structural geology (Oda, 1984):

$$\mathbf{F} = \frac{\boldsymbol{\pi}}{4} \frac{N}{V_{REV}} \int_0^{\infty} \int_{\boldsymbol{\Omega}} r^3 \bar{E}\left(r, \mathbf{n}\right) \mathbf{n} \otimes \mathbf{n} \ d\mathbf{n} dr$$

2.

In which $\bar{E}\left(r, \mathbf{n}\right)$ is the mathematical expectancy of the presence of a crack of radius r and normal direction $\boldsymbol{n}$ in a REV of size V_{REV}. A direct relationship can be established between fabric tensors and rock stiffness tensor (Cowin, 1985; Lubarda and Krajcinovic, 1993). The key issue is to choose relevant microstructure descriptors (Lu and Torquato, 1992; Lecampion, 2010) and associated probability density functions (pdf).

2.3.2. Continuum-based, thermodynamic models

At the scale of the REV, the first law of thermodynamics writes:

$$W_{ext} = \mathbf{\Pi} + Q + U_i$$

3.

In which W_{ext} is the work supplied by external forces, Π is the potential energy stored in the REV (including: the potential for elastic deformation and the potential for surface energy release during crack opening), Q is the heat transmitted to the REV under the action of the external forces, and U_i is the energy dissipated due to irreversible microstructure changes within the REV. In the absence of microstructure changes, damage is work-conjugate to the energy release rate (noted $\boldsymbol{Y}$ and also called affinity in fracture mechanics) through the potential energy. However, if microstructure changes occur in the REV, the stored potential energy of the rock is not entirely available for the creation of additional material surfaces. Assuming for instance that the driving force responsible for irreversible microstructure changes is proportional to the deformation ($g_M\boldsymbol{\varepsilon}$) (Swoboda and Yang, 1999):

$$-\frac{\partial \mathbf{\Pi}}{\partial \mathbf{D}} \neq \mathbf{Y}, \quad -\frac{\partial \mathbf{\Pi}}{\partial \mathbf{D}} = \mathbf{Y} + g_M \boldsymbol{\varepsilon}$$

4.

In the following, g_M is called the “resistance to crack closure”, because $-g_M\boldsymbol{D}$ actually represents the amount of compression stress needed to completely close cracks open in tension - in addition to the “compression” associated to the relaxation of tensile stress. As a result, the expression of the free energy of the rock solid skeleton is sought in the form:

$$\mathbf{\Psi} = \mathbf{\Pi} - g_M \boldsymbol{\varepsilon} : \mathbf{D}$$

5.

The Continuum Damage model formulation described above relies on a minimal number of energetic postulates, since the flow of irreversible deformation associated to microstructure changes depends on the damage flow rule (Arson and Gatmiri, 2012). The expressions of the free energy, the damage criterion and the damage potential are the only three requirements needed to close the formulation (in fact only two postulates are needed for associate flow rules, for which the damage potential is equal to the damage yield function). The low number of functions postulated in the model is expected to reduce the number of material parameters needed to describe crack-induced anisotropy in stiffness and deformation. Even so, model calibration by experimental stress/strain curves is not straightforward: each new data point adds as many equations as additional unknowns, so that the calibration process as a whole requires an iterative procedure (Xu et al., 2013).

3. Rock Damage Prediction Method: CDM and the Bayesian Paradigm

3.1. Uncertainty Quantification of Damage Predictions

It is proposed herein to couple the Finite Element Method to a probabilistic computational engine in order to overcome model formulation and calibration problems encountered in damage rock mechanics. To illustrate the methodology, simulations were performed by using the "THHMD" Continuum Damage Mechanics model (Arson and Gatmiri, 2010; 2012) implemented in Theta-Stock Finite Element program (Gatmiri and Arson, 2008). The damage variable is defined as the second-order crack density tensor (equation 1). The main thermodynamic postulates at the foundation of the THHMD model are summarized in Table 1.

Table 1. Mechanical constitutive equations in the THHMD model (Arson and Gatmiri, 2012).

The free energy follows the form of equation 5. For a purely mechanical problem (no capillary or thermal effects), stress is written as:

$$\boldsymbol{\sigma} = \frac{\partial \boldsymbol{\psi}(\boldsymbol{\varepsilon}, \mathbf{D})}{\partial \boldsymbol{\varepsilon}} = \mathbf{C}(\mathbf{D}) : \boldsymbol{\varepsilon} - g_M \mathbf{D}$$

6.

For instance, if damage is induced by tensile stress, a bare unloading to zero tensile stress will not produce a state of zero-deformation. To close all the cracks open due tensile damage, it is necessary to apply a compression stress equal to $-g_M \boldsymbol{D}$. The principle of strain decomposition adopted in the THHMD model is illustrated in Figure 1.

Figure 1. Sketch of a typical stress-strain curve predicted with the THHMD model for a purely mechanical problem. Deformation is decomposed into three components: (1) the purely elastic strain ($\varepsilon^{\mathrm{el}}$), which would be obtained in the absence of damage, (2) the additional elastic deformation ($\varepsilon^{\mathrm{ed}}$) induced by the reduction of stiffness with damage, and (3) the irreversible deformation resulting from the residual crack opening ($\varepsilon^{\mathrm{id}}$). E_{ref} denotes the reference Young's modulus, and E(D) is the damaged Young's modulus.

Because the damage variable represents the average volume occupied by cracks in the principal directions of stress, the THHMD variable does not capture non-local mechanical effects. However, the g_M parameter may be viewed as a scaling parameter similar to an internal length (Arson and Gatmiri, 2008). Moreover, the computation of the damaged permeability tensor requires some assumptions on rock fabric (such as the ratio between crack aperture and crack length), and a relationship has to be established between crack density and crack geometric parameters. As a result, damaged permeability in the THHMD model is scaled by the REV size. The consequent mesh dependency observed for permeability in FEM needs to be regularized in order to capture the inherent non-local effects of micro-crack propagation on REV

flow properties (Arson, 2012). Relating pore and crack size distributions to intrinsic permeability provides the necessary multi-scale framework to do so (Arson and Pereira, 2013), but further developments are needed to properly relate macroscopic percolation thresholds to micro-crack connectivity. The following probabilistic calibration focuses on mechanical damage parameters. Only the mechanical degrees of freedom were activated in the simulations performed with Theta-Stock.

The Finite Element algorithm of the THHMD model was incorporated in a computation code dedicated to probabilistic modelling (Medina-Cetina et al., 2007). Four damage parameters (listed in detail below) were considered as random variables, and two types of simulations were performed:

1. *Case I: no observation data is available (forward problem).* Probability density functions were assigned to the random variables, according to "expert's judgement" - even when there is no existing evidence or previous experience on the use of one particular parameter, it is always possible to assign a non-informative probability distribution to it. Model performance was assessed from the predictions obtained while solving the "forward problem", using Monte-Carlo simulations.
2. *Case II: experimental data is made available (inverse problem)*. The Bayesian theory was used to update the model parameters.

3.2. Probabilistic Calibration via the Bayesian Paradigm

One of the major challenges for the implementation of geomechanical models is the proper characterization of the model's parameters. In practice, the parameterization of advanced geomechanical models is commonly formulated as an optimization problem, where an objective function is defined to minimize the trade-off between the experimental observations and the corresponding model predictions. The result is given in the form of a single vector of model parameters –containing the "optimal" set of parameters. Furthermore, most of the current calibration processes imply that the data used to define the optimal set of model parameters is fully certain, and that the amount and location (in space and time) of data used for the calibration has no impact on the selection of the model parameters. It is also common to disregard the uncertainty carried by the model predictions due to inherent limitations on the theory supporting it, providing little ground to define the optimal degree of model complexity. That is the reason why it is proposed to use the Bayesian paradigm (Medina-Cetina, 2006) to calibrate the parameters of the THHMD model introduced above. The Bayesian approach makes inferences founded on statements that convey the integration of two main sources of information: the *prior*, derived from previous knowledge about the parameters; and the *likelihood*, based on the inferences assimilated by the data itself. Both of these are expressed in the form of probability density functions, which combined give a conditional joint probability function called *posterior*, which is itself the solution to the co-called "inverse problem". The Bayes' theorem defines the solution to the inverse problem as (Robert and Casella, 2004):

$$\boldsymbol{\pi}\left(\boldsymbol{\theta}|\mathbf{d}_{\mathbf{obs}}\right)=\frac{f\left(\mathbf{d}_{\mathbf{obs}}|\boldsymbol{\theta}\right)\boldsymbol{\pi}\left(\boldsymbol{\theta}\right)}{\int f\left(\mathbf{d}_{\mathbf{obs}}|\boldsymbol{\theta}\right)\boldsymbol{\pi}\left(\boldsymbol{\theta}\right)d\boldsymbol{\theta}}$$

7.

In which $\boldsymbol{d_{obs}}$ is a vector containing observations, $\boldsymbol{\theta}$ is the sought vector of model parameters, $\boldsymbol{\pi}\left(\boldsymbol{\theta}\right)$ is the *prior*, $f\left(\mathbf{d}_{\mathbf{obs}}|\boldsymbol{\theta}\right)$ is the *likelihood* ; and $\boldsymbol{\pi}\left(\boldsymbol{\theta}|\mathbf{d}_{\mathbf{obs}}\right)$ is the *posterior*. The integration of the *posterior* becomes a challenge for a multivariate and multi-level Bayesian definition due to the number of samples needed to converge to the target joint probability density function of $\boldsymbol{\theta}$. To overcome this problem, it is proposed to use the Markov Chain Monte Carlo (MCMC) method, which is a numerical procedure that allows for the sampling of a *posterior*. An important property of the MCMC method is that it converges to the target joint density as the sample grows. The decision rule that selects the samples is the Metropolis-Hastings rule (M-H), which is a generalized form of the Metropolis and Gibbs methods (Robert and Casella, 2004). It is worth noticing that the added value on the calibration of constitutive models relies on the efficient implementation of the Bayesian inference to assess first and second order statistics from the posterior, which leads to a systematic and reliable performance assessment of the proposed model. Moreover, any changes or 'interventions' executed after the probabilistic calibration are now traceable by comparing the effect of the 'updating' feature of the Bayesian paradigm (e.g. after increasing the model complexity, the mesh resolution, or adding more experimental observations).

4. Results

4.1. Description of the Calibration Problem

A triaxial compression test performed on sandstone was simulated. Zero vertical displacements were imposed at the bottom (fixed basis), and zero lateral displacements were imposed along the axis of the sample (axis-symmetric conditions). The confining pressure was first raised from 0 to 15 MPa on both the lateral and top external boundaries (isotropic confining phase). Then, the confining pressure was maintained at the external lateral boundary, while the axial stress was increased up to failure at the top boundary. Observation data used for "Case II" described above consisted of experimental stress/strain curves reported in (Dragon et al., 2000). For simplicity, the applicability of the probabilistic method described above was tested for experimental observations $\mathbf{d}_{obs}$ that consisted of points taken from the plot of stress against axial strain curve only. It is anticipated that the inclusion of data points from the volumetric strain curve would modify the posterior and reduce the uncertainty of the model performance. However, there is in general little experimental evidence on the variability of the volumetric response of geomaterials, which makes it challenging to determine an informative covariance in the likelihood function. A hyper-parameter addressing the unknown degree of variability of the volumetric response would actually have to be defined. This latter analysis is out of the scope of this paper, but it will be considered in future investigations by the authors. Note that even if volumetric strains were not included in the observation data used for the probabilistic calibration, the THHMD model can capture anisotropic damage effects on stiffness and deformation in sandstone subjected to triaxial compression loading, and predict the subsequent crack-induced dilatant behaviour of damaged rock (e.g., Arson and Gatmiri, 2011). Figure 2 gathers stress-strain plots obtained with the THHMD model that were fitted to the experimental data used as prior in the proposed analysis, before performing the probabilistic calibration. Numerical results show that under axial compression, cracks open in planes containing the axial direction of loading: crack opening induce tensile strains in the radial direction and compression strain in the axial direction. Overall, compression-induced damage results in an increase of REV volume, i.e., in dilatant volumetric deformation.

Figure 2. Triaxial Compression Test performed on Sandstone under a Confining Pressure of 15 MPa. Plot of Axial, Radial and Volumetric Deformation against Deviatoric Stress: (1) Obtained in the Experiment Reported in (Dragon et al., 2000) – dots; (2) Obtained by Finite Element Simulation with the THHMD Model Before Probabilistic Calibration – solid lines.

4.2. Solution of the Forward and Inverse Problems

In all the simulations presented in this paper, the Poisson's ratio of the undamaged material was taken equal to 0.2 (according to Dragon et al., 2000). Four material parameters were set as random variables: Young's modulus of the undamaged sandstone (E), the mechanical resistance to crack closure (g_M), the initial threshold required to trigger damage (C_0) and the

hardening parameter (C_1). The corresponding probability density functions are provided in Table 2. Note that the stress/strain curves shown in Figure 2 actually illustrate the behaviour of sandstone for the mean values of the constitutive parameters of interest.

Table 2. Probability Density Functions (P.D.F.) assigned to the Damage Parameters (Random Variables R.V.)

The forward problem (Case I, expert's judgment) and the inverse problem (Case II, experimental observations) were solved for 7,000 realizations of the model, with the vector of model parameters defined as: $\theta = \{E, g_M, C_0, C_1\}$. When comparing results from the solution of both problems, it is observed that "informing" the damage model with experimental data strongly influences the cumulative probability density functions of Young's modulus, the resistance to crack closure, and the damage "hardening parameter" (Fig.3.a, b & d): in "Case II", the probability density functions of E, g_M, *and* C_1 show indeed a significant reduction on uncertainty (i.e. cumulative probability density functions exhibit steeper slopes). On the other hand, the prediction of the initial damage threshold C_0 does not seem to be affected by the observation data introduced in the Bayesian method in terms of uncertainty reduction (Fig.3.c): the probability density function of C_0 gets only shifted to higher values. Mechanically speaking, this means that the energy that needs to be released to initiate crack propagation is contingent upon conditions external to the model - the initial texture of the rock for instance. In summary, the analysis of the cumulative probability functions shows that in general, the introduction of experimental observations improves model predictions and reduces the uncertainty on the value of the model parameters. As a result, the bundle of stress/strain curves obtained for Case II is contained in a narrower band than for Case I (Figure 4).

Figure 3. Cumulative density functions of the random variables studied in the present damage model analysis. *Case I refers to the forward problem (based on experts' judgement). Case II refers to the inverse problem (using experimental data).*

Figure 4. Stress/strain predictions for the triaxial compression test simulated (deviatoric stress versus axial deformation). *Dots represent the observation data taken from (Dragon et al., 2000). Solid lines are the numerical predictions obtained in the forward problem.*

4.3. Parameter Correlations

One of the most striking benefits of the use of the Bayesian paradigm to solve the inverse problem is the possibility to retrieve the correlation structure between the model parameters. The physical interpretation of the correlations obtained while solving the inverse problem is explained below.

4.2.1. Joint probability of E and g_M (Fig.5.a).

For a given state of stress, tensile strains are expected to be higher for lower values of Young's modulus. To get the same damage predictions, a decrease of Young's modulus has to be compensated by a decrease of the absolute value of g_M (see the expression of the damage function in Tab.1). In addition, tensile strains should be inversely proportional to E and g_M (by construction of the model). Therefore a linear correlation is expected between E and g_M. The results shown in Fig.5.a. are in agreement with this statement, especially for low values of Young's modulus (ρ=0.3), i.e. for weaker materials.

4.2.2. Joint probability of E and C_1 (Fig.5.b).

The stress boundary conditions are fixed in the problem. Therefore, if E is decreased (with a variable C_1), the amount of damage measured in the experiment can only be predicted accurately if C_1 is increased. Physically, this means that it is easier to damage the sample as E gets smaller, but this effect can be compensated by rock hardening (when C_1 gets higher). The resulting correlation between E and C_1 is linear, for the same reasons as above (for E and g_M).

4.2.3. Joint probability of g_M and C_1 (Fig.5.c).

The correlation between E and g_M on the one hand, and between E and C_1 on the other hand, justify the correlation between g_M and C_1 observed in Fig.5.c. Indeed, increasing the value of the resistance to crack closure g_M increases the probability of damage propagation. This effect is compensated by damage propagation itself (controlled by parameter C_1): a weaker, damaged material is less brittle than the virgin material.

Figure 5. Relative Frequency Maps of the correlated random variables: (a) Young's modulus E and resistance to crack closure g_M; (b) Young's modulus E and hardening parameter C_1; (c) resistance to crack closure g_M and hardening parameter C_1.

4.2.4. Correlations between C_0 and the other parameters under study (Fig.6).

C_0 only controls the initiation of damage. Once the material has started to crack, the evolution of damage is controlled by g_M, C_1 and elastic parameters (Young's modulus, Poisson's ratio). Figure 6 shows that indeed, there is no correlation between C_0 and the three other material parameters studied in this example.

Figure 6. Relative Frequency Maps showing the absence of correlation between the initial damage threshold C_0 and: (a) the hardening parameter C_1; (b) Young's modulus E; (c) the resistance to crack closure g_M.

5. Conclusions

A probabilistic approach was adopted to calibrate a Continuum Damage Mechanics model suitable for rocks. The constitutive equations derive from a postulated free energy potential, capturing changes of stiffness and deformation due to crack propagation. Four damage parameters were set as random variables to simulate a triaxial compression test: Young's modulus E, the resistance to crack-closure g_M, the initial damage threshold, C_0 and the hardening parameter C_1. Two sets of realizations of $\theta = \{E, g_M, C_0, C_1\}$ were generated: (1) first by solving the forward problem (Case I), in which the probability density functions used for the random variables are chosen according to expert's judgement; (2) second, by solving the inverse problem (Case II), in which experimental observations are made available for the updating of the parameters definitions. Results confirm that introducing evidence from experimental observations in the calibration process increases the model performance and reduces the uncertainty of the predictions.

Developing efficient computational tools to predict damage is critical to diagnose structural failures or to make technical recommendations about retro-fitting practices. The behaviour of geomaterials used in construction (rock and concrete for instance) requires complex constitutive models, accounting for diverse types of discontinuities and material heterogeneities. This research work aims to minimize the number of postulates and model parameters involved in damage models. Joint probability maps presented in this paper highlight the correlations between parameters E, g_M and C_1 (respectively: Young's modulus of the virgin material, resistance to crack closure, and hardening parameter). These correlations result from the form of the damage evolution function and indicate that a similar accuracy in the prediction of damage might be achievable with less than three parameters. C_0 (the initial damage threshold) influences damage initiation, but does not play any role in damage growth, which explains the absence of correlation between C_0 and the other parameters. Mechanically speaking, this means that the energy that needs to be released to initiate crack propagation is contingent upon conditions external to the model - the initial texture of the rock for instance. Therefore it may be necessary to complement mechanical loading tests by microstructure observation to fully characterize the geomaterials used in construction or reparation.

References

Arson, C. (2012). Using a geo-mechanical damage model to assess permeability in cracked porous media: internal length parameter issues, Special Topics & Reviews in Porous Media, 3(1):69-77

Arson, C. and Gatmiri, B. (2008). On damage modelling in unsaturated clay rocks, Physics and Chemistry of the Earth, 33:S407–S415

Arson, C. and Gatmiri, B. (2010). Numerical study of a thermo-hydro-mechanical damage model for unsaturated porous media. Annals of Solid and Structural Mechanics, 1:59–78.

Arson, C. and Gatmiri, B. (2011). Numerical Study of Damage in Unsaturated Geological and Engineered Barriers, Physics and Chemistry of the Earth, 36:1981-1989

Arson, C. and Gatmiri, B. (2012). Thermo-Hydro-Mechanical Modeling of Damage in Unsaturated Porous Media: Theoretical Framework and Numerical Study of the EDZ, International Journal for Numerical and Analytical Methods in Geomechanics, 36:272-306

Arson, C. and Pereira, J.-M. (2013). Influence of Damage on Pore Size Distribution and Permeability of Rocks, International Journal for Numerical and Analytical Methods in Geomechanics, 37:810-831

Arson, C., Xu, H. and Chester, F.M. (2012). On The Definition Of Damage In Time-Dependent Healing Models For Salt Rock, Géotechnique Letters, 2:67-71

Auqué LF, Acero P, Gimeno MJ, Gomez JB, Asta MP. (2009). Hydrogeochemical Modeling of a Thermal System and Lessons Learned for CO2 Geologic Storage. Chemical Geology, **268**:324**–**336.

Blumling P, Bernier F, Lebon P, Martin CD. (2007). The excavation damaged zone in clay formations time-dependent behaviour and influence on performance assessment. Physics and Chemistry of the Earth, 32(8**–**14):588**–**599.

Blunt, M.J. (2001). Flow in Porous Media – Pore-Network Models and Multiphase Flow, Current Opinion in Colloid & Interface Sciences, 6:197-207

Bonin B. (1998). Deep geological disposal in argillaceous formations: studies at the Tournemire test site. Journal of Contaminant Hydrology, 35:315**–**330.

Bera B, Bera M, Sushanta K, Vick D. (2011). Understanding the micro structure of Berea Sandstone by the simultaneous use of micro-computed tomography (micro-CT) and focused ion beam-scanning electron microscopy (FIB-SEM). Micron, 42(5):412**–**418

Cauvin, A. and Testa, R.B. (1999). Damage mechanics: basic variables in continuum theories. International Journal of Solids and Structures, 36:747-761

Chaboche, J.-L. (1992). Damage Induced Anisotropy: On the Di_culties Associated with the Active/Passive Unilateral Condition. International Journal of Damage Mechanics, 1:148-171.

Chan KS, Bodner SR, Munson DE. (2001). Permeability of WIPP Salt during Damage Evolution and Healing. International Journal of Damage Mechanics, 10:347**–**375.

Cosenza P, Ghoreychi M, Bazargan-Sabet B, de Marsily G. (1999). In situ rock salt permeability measurement for long-term safety assessment of storage. International Journal of Rock Mechanics and Mining Sciences, 36(4):509–526

Cowin, S.C. (1985). The relationship between the elasticity tensor and the fabric tensor. Mechanics of Materials, 4:137-147

Dormieux, L., Kondo, D. and Ulm, F.-J. (2006). A micro mechanical analysis of damage propagation in fluid-saturated cracked media. C.R. Mécanique, 334: 440-446.

Dragon, A., Halm, D. and Désoyer, T. (2000). Anisotropic damage in quasi-brittle solids : modelling, computational issues and applications. Comput. Methods Appl. Mech. Engrg., 183:331–352.

Durner W. (1994). Permeability estimation for soils with heterogeneous pore structure. Water Resources Research, 30(2):211–223

Garcia-Bengoechea I, Lovell CW and Altschaeffl AG. (1979). Pore distribution and permeability of silty clays. Journal of the Geotechnical Engineering Division, 105:839–856

Gatmiri, B. and Arson, C. (2008). Theta-Stock, a powerful tool for thermohydromechanical behaviour and damage modelling of unsaturated porous media. Computers and Geotechnics, 35(6):890-915.

Gens A, Garcia-Molina AJ, Olivella S, Alonso EE, Huertas F. (1998). Analysis of a full scale in situ test simulating repository conditions. International Journal for Numerical and Analytical Methods in Geomechanics, 22:515–548.

Guéguen, Y., Gravilenko, P. and Le Ravalec, M. (1996). Scales of Permeability, Surveys in Geophysics, 17:245-263

Halm, D. and Dragon, A. (1998). An anisotropic model of damage and frictional sliding for brittle materials. Engineering Fracture Mechanics, 25:729-737.

Homand F, Chiarelli AS, Hoxha DD. (2002). Caractéristiques physiques et mécaniques du granite de la Vienne et de l'argilite de l'Est. Revue Française de Génie Civil, 6(1):11–20.

Kachanov, M. (1992). Effective elastic properties of cracked solids: critical review of some basic concepts. Appl. Mech. Rev., 45(8):304–335

Lecampion, B. (2010). Stress-induced crystal preferred orientation in the poromechanics of in-pore crystallization. Journal of the Mechanics and Physics of Solids, 58:1701-1715

Levasseur, S., Collin, F., Charlier, R. and Kondo, D. (2011). A two-scale anisotropic damage model accounting for initial stresses in microcracked materials. Engineering Fracture Mechanics, 78(9):1945-1956

Lu, B. and Torquato, S. (1992). Nearest-surface distribution functions for poly-dispersed particle systems. Physical Review A, 45(8):5530-5544

Lubarda, V.A. and Krajcinovic, D. (1993). Damage tensors and the crack density distribution. International Journal of Solids and Structures, 30(20):2659-2677

Maleki, K. and Pouya, A. (2010). Numerical simulation of damage–Permeability relationship in brittle geomaterials, Computers and Geotechnics, 37:619-628

Martino JB, Chandler NA. (2004). Excavation-induced damage studies at the Underground Research Laboratory. International Journal of Rock Mechanics and Mining Sciences, 41:1413–1426.

Medina-Cetina, Z. (2006). Probabilistic Calibration of Soil Constitutive Models, Dissertation, Philosophy Doctor, The Johns Hopkins University, Baltimore MD

Medina-Cetina Z., Ghanem R. and Rechenmacher A. (2007). A Functional Bayesian Method for the Solution of Inverse Problems with Spatio-Temporal Parameters, 6th European LS_DYNA Users Conference, Gothenburg Sweden, May 29-30

Oda, M. (1984). Similarity rules of crack geometry in statistically homogeneous rock masses. Mechanics of Materials, 3:119-129

Pensée, V., Dormieux, L. and Kondo, D. (2002). Micro-mechanical Analysis of Anisotropic Damage in Brittle Materials. C.R. Journal of Engineering Mechanics, 128(8): 889-897.

Raj, R. (1982). Creep in Polycrystalline Aggregates by Matter Transport Through a Liquid Phase, Journal of Geophysical Research, 87(B6):4731-4739

Rieu, M. and Sposito, G. (1991). Fractal Fragmentation, Soil Porosity, and Soil Water Properties: I. Theory, Soil Sci. Soc. Am. J., 55:1231-1238

Robert, C.P. and Casella, G. (2004). Monte Carlo Statistical Methods. Springer, New York

Romero, E. and Jommi, C. (2008). An insight into the role of hydraulic history on the volume changes of anisotropic clayey soils. Water Resources research, 44, W12412 (16 pages)

Schubnel, A., Benson, P., Thompson, B., Hazzard, J. and Young, R. (2006). Quantifying damage, saturation and anisotropy in cracked rocks by inverting elastic wave velocities, Pure Appl. Geophys. 363:947-973.

Senseny, P.E., Hansen, F.D. Russell, J.E., Carter, N.L., Handin, J.W. (1992). Mechanical Behaviour of Rock Salt: Phenomenology and Micromechanisms, Int. J. Rock Mech. Min. Sci. & Geomech. Abstr, 29(4):363-378

Shao, J.-F., Zhou, H. and Chau, K.T. (2005). Coupling between anisotropic damage and permeability variation in brittle rocks. International Journal for Numerical and Analytical Methods in Geomechanics, 29:1231–1247.

Slizowski J, Walaszczyk J. Long (2008). term stability evaluation of natural gas storage caverns. Mineral Resources Management, 24(4–1):83–100.

Souley M, Homand F, Pepa S, Hoxha D. (2001). Damage-induced permeability changes in granite: a case example at the URL in Canada. International Journal of Rock Mechanics and Mining Sciences, 38:297–310.

Spiers, C.J., Schutjens, P.M., Brzesowsky, R.H., Peach, C.J., Liezenberg, J.L., Zwart, H.J. (1990). Experimental determination of constitutive parameters governing creep of rocksalt by pressure solution, in: Deformation Mechanisms, Rheology and Tectonics, Geological Society Special Publication, 54, 215-227.

Swoboda, G. and Yang, Q. (1999). An energy-based damage model of geomaterials 1. Formulation and numerical results. Int. J. Solids and Struct., 36:1719–1734

Tsang CF, Bernier F, Davies C. (2005). Geohydromechanical processes in the Excavation Damaged Zone in crystalline rock, rock salt, and indurated and plastic clays - in the context of radioactive waste disposal. International Journal of Rock Mechanics and Mining Sciences, 42:109–125.

Van Genuchten, MT. (1980). A closed-form equation for predicting the permeability of unsaturated soils. Soil Science Society of America Journal, 44:892–898

Vogel T, Gerke HH, Zhang R, and Van Genuchten MT. (2000).Modeling flow and transport in a two-dimensional dual-permeability system with spatially variable hydraulic properties. Journal of Hydrology, 238:78–89

Xu T, Apps JA, Pruess K. (2004). Numerical Simulation of CO2 Disposal by Mineral Trapping in Deep Aquifers. Applied Geochemistry, 19:917–936.

Xu, H., Arson, C. and Busetti, S. (2013). Modeling the Anisotropic Damaged Zone Around Hydraulic Fractures: Thermodynamic Framework and Simulation of Mechanical Tests, 47th US Rock Mechanics/Geomechanics Symposium of the American Rock Mechanics Association, San Francisco, CA, 23-25 June 2013, paper ID: 13-375

Zangeneh, N., Eberhardt, E. and Bustin, R.M. (2012). Application of the distinct-element method to investigate the influence of natural fractures and in-situ stresses on hydrofrac propagation, 46th US Rock Mechanics/Geomechanics Symposium of the American Rock Mechanics Association, Chicago, IL, 23-26 June 2013, paper ID: 12-223

Zhu, C. and Arson, C. (2014). A Thermo-Mechanical Damage Model for Rock Stiffness during Anisotropic Crack Opening and Closure, Acta Geotechnica (in press)

Zhu Q., Kondo, D., Shao, J.-F. (2007). An Homogenization-Based Nonlocal Damage Model for Brittle Materials and Applications. ICCS 2007, Part III, LNCS 4489, Springer-Verlag, Shi et al. (eds), 1130-1137.

Zimmermann, G., Burkhardt, H. and Engelhard, L. (2003). Scale Dependence of Hydraulic and Structural Parameters in the Crystalline Rock of the KTB, Pure Appl. Geophys., 160:1067-1085

Figure captions

Figure 1. Sketch of a typical stress-strain curve predicted with the THHMD model for a purely mechanical problem. Deformation is decomposed into three components: (1) the purely elastic strain ($\varepsilon^{\mathrm{el}}$), which would be obtained in the absence of damage, (2) the additional elastic deformation ($\varepsilon^{\mathrm{ed}}$) induced by the reduction of stiffness with damage, and (3) the irreversible deformation resulting from the residual crack opening ($\varepsilon^{\mathrm{id}}$). E_{ref} denotes the reference Young's modulus, and E(D) is the damaged Young's modulus.

Figure 2. Triaxial Compression Test performed on Sandstone under a Confinement Pressure of 15 MPa. Plot of Axial, Radial and Volumetric Deformation against Deviatoric Stress: (1) Obtained in the Experiment Reported in (Dragon et al., 2000) – dots; (2) Obtained by Finite Element Simulation with the THHMD Model Before Probabilistic Calibration – solid lines.

Figure 3. Cumulative density functions of the random variables studied in the present damage model analysis. *Case I refers to the forward problem (based on expert's judgement). Case II refers to the inverse problem (using experimental data).*

- **a.** Young's modulus *E*.
- **b.** Resistance to crack closure g_M.
- **c.** Initial damage threshold C_0.
- **d.** Damage hardening parameter C_1.

Figure 4. Stress/strain predictions for the triaxial compression test simulated (deviatoric stress versus axial deformation). *Dots represent the observation data taken from (Dragon et al., 2000). Solid lines are the numerical predictions obtained in the forward problem.*

a. Case I (expert's judgement).
b. Case II (experimental data).

Figure 5. Relative Frequency Maps of the correlated random variables: (a) Young's modulus *E* and resistance to crack closure g_M; (b) Young's modulus *E* and hardening parameter C_1; (c) resistance to crack closure g_M and hardening parameter C_1.

Figure 6. Relative Frequency Maps showing the absence of correlation between the initial damage threshold C_0 and: (a) the hardening parameter C_1; (b) Young's modulus *E*; (c) the resistance to crack closure g_M.

Table 1. Mechanical constitutive equations in the THHMD model (Arson and Gatmiri, 2012).

Functional	**Postulated Expression**
Free Energy ψ	$\boldsymbol{\psi}\left(\boldsymbol{\varepsilon},\mathbf{D}\right)=\frac{1}{2}\boldsymbol{\varepsilon}:\mathbf{C}\left(\mathbf{D}\right):\boldsymbol{\varepsilon}-g_M\boldsymbol{\varepsilon}:\mathbf{D}$
Damage function f_d	$f_d\left(\boldsymbol{\varepsilon},\mathbf{Y}_1^+\right)=\sqrt{\frac{1}{2}\mathbf{Y}_1^+:\mathbf{Y}_1^+}-C_0-C_1Tr\left(\mathbf{D}\right),\quad \mathbf{Y}_1^+=-g_M\boldsymbol{\varepsilon}^+$
Deformation Component	**Definition**
Purely Elastic ε^{el} with: $\varepsilon^{E}=\varepsilon^{el}+\varepsilon^{ed}$	$\boldsymbol{\varepsilon}^{el}=\mathbf{C}_{\mathbf{ref}}^{-1}:\boldsymbol{\sigma}$
Elastic Damaged ε^{ed}	$\boldsymbol{\varepsilon}^{ed}=\left[\mathbf{C}\left(\mathbf{D}\right)^{-1}-\mathbf{C}_{\mathbf{ref}}^{-1}\right]:\boldsymbol{\sigma}$
Irreversibly damaged ε^{id}	$\boldsymbol{\varepsilon}^{id}=\mathbf{C}\left(\mathbf{D}\right)^{-1}:\left(-g_M\mathbf{D}\right)$

$\boldsymbol{C_{ref}}$: stiffness tensor of the virgin material (prior to loading). ***C(D):*** damaged stiffness tensor

C_0: initial damage threshold, C_1: hardening parameter, g_M: resistance to crack closure

Table 2. Probability Density Functions (P.D.F.)
assigned to the Damage Parameters (Random Variables R.V.)

R.V.	P.D.F.	Mean	Std. Deviation	Min.	Max.
E	normal	11.4 GPa	0.13 GPa	11.2 GPa	1220 GPa
g_M	modified exponential	-30 MPa	0.07 MPa	-33 MPa	0 MPa
C_0	log-normal	20 kPa	1.00	8.1 kPa	
C_1	log-normal	274 kPa	9.0	260 kPa	32 MPa

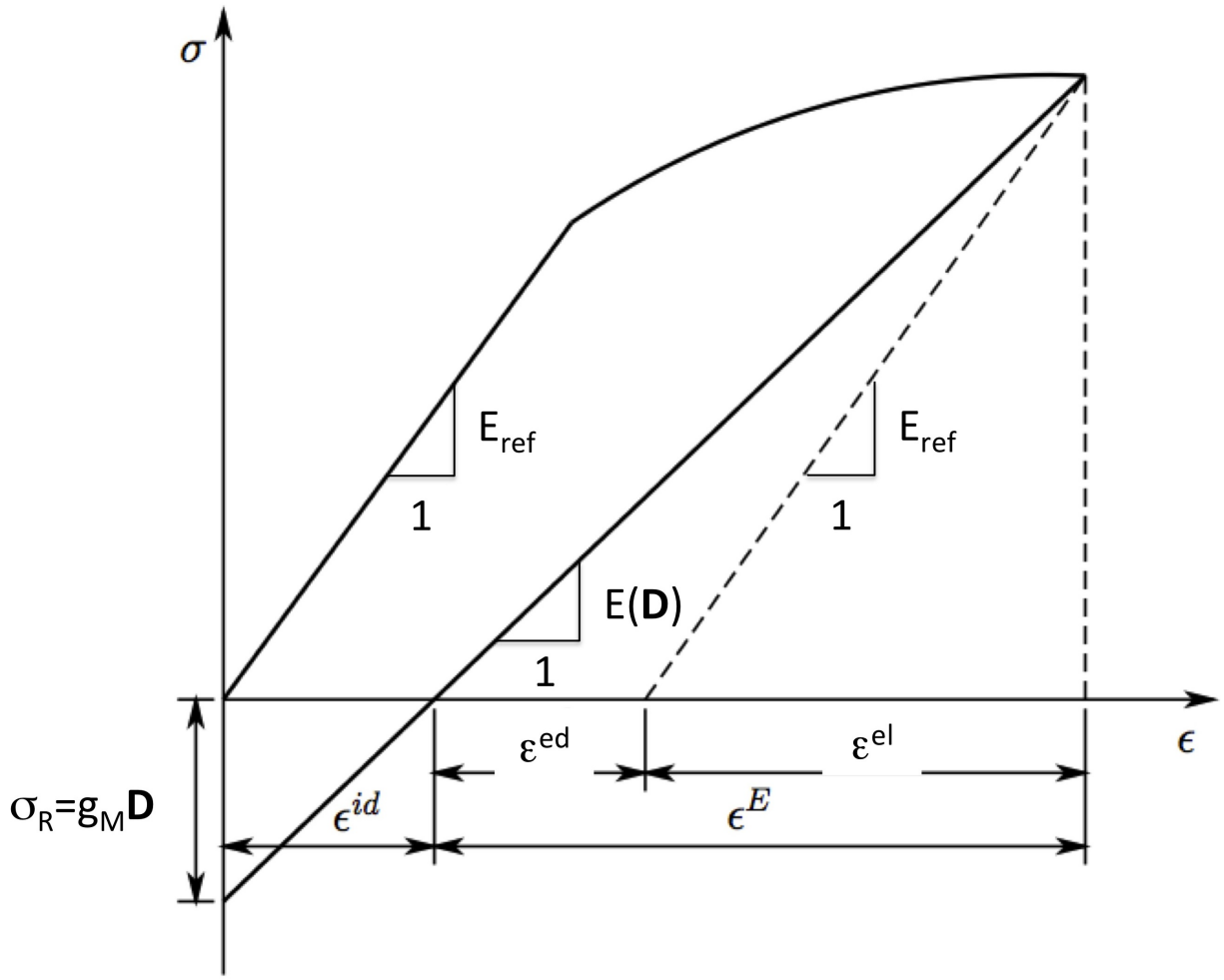

Figure 1:

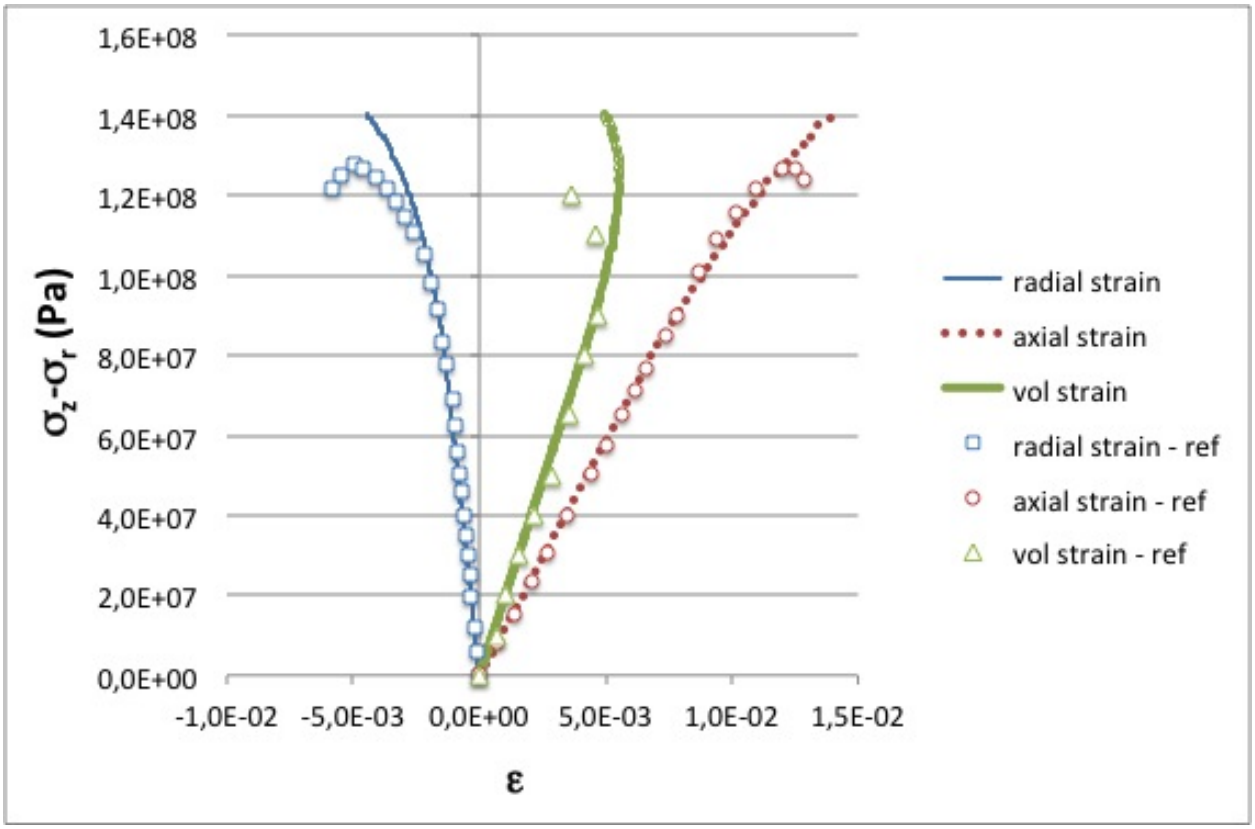
1,6E+08
1,4E+08
1,2E+08
1,0E+08
8,0E+07
6,0E+07
4,0E+07
2,0E+07
0,0E+00
σz-σr (Pa)
-1,0E-02
-5,0E-03
0,0E+00
5,0E-03
1,0E-02
1,5E-02
ε
radial strain
axial strain
vol strain
radial strain - ref
axial strain - ref
vol strain - ref

Figure 2:

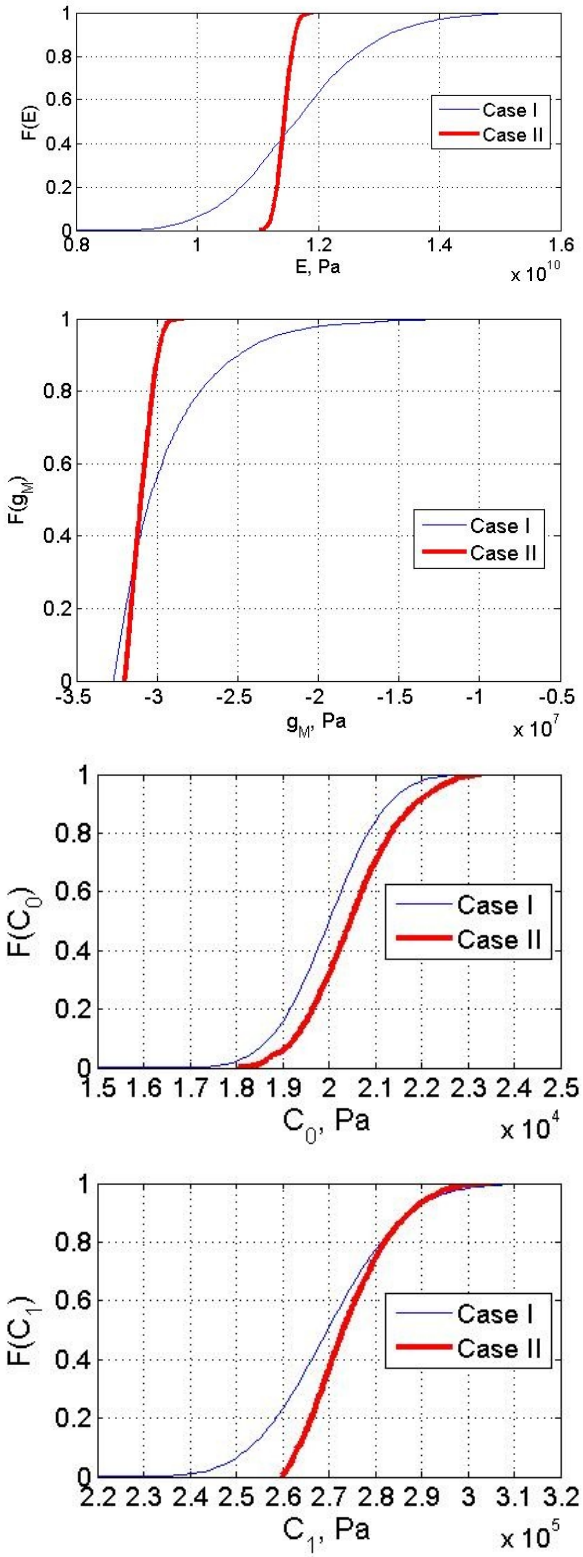
F(E)
E, Pa
x 10^10
Case I
Case II
F(g_M')
g_M', Pa
x 10^7
F(C_0)
C_0, Pa
x 10^4
F(C_1)
C_1, Pa
x 10^5

Figure 3:

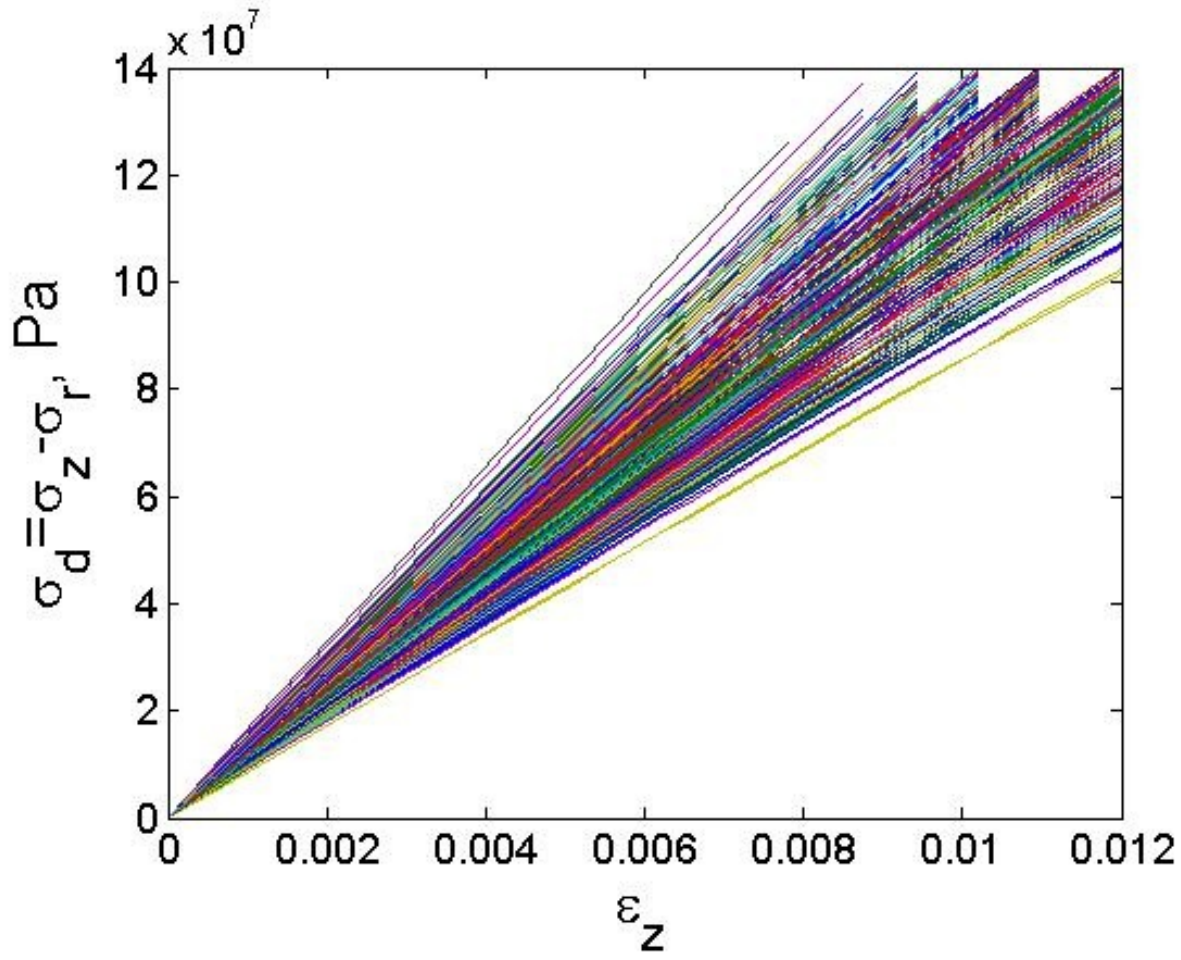
x 10^7
14
12
10
8
6
4
2
0
0
0.002
0.004
0.006
0.008
0.01
0.012
σd=σz-σr, Pa
εz

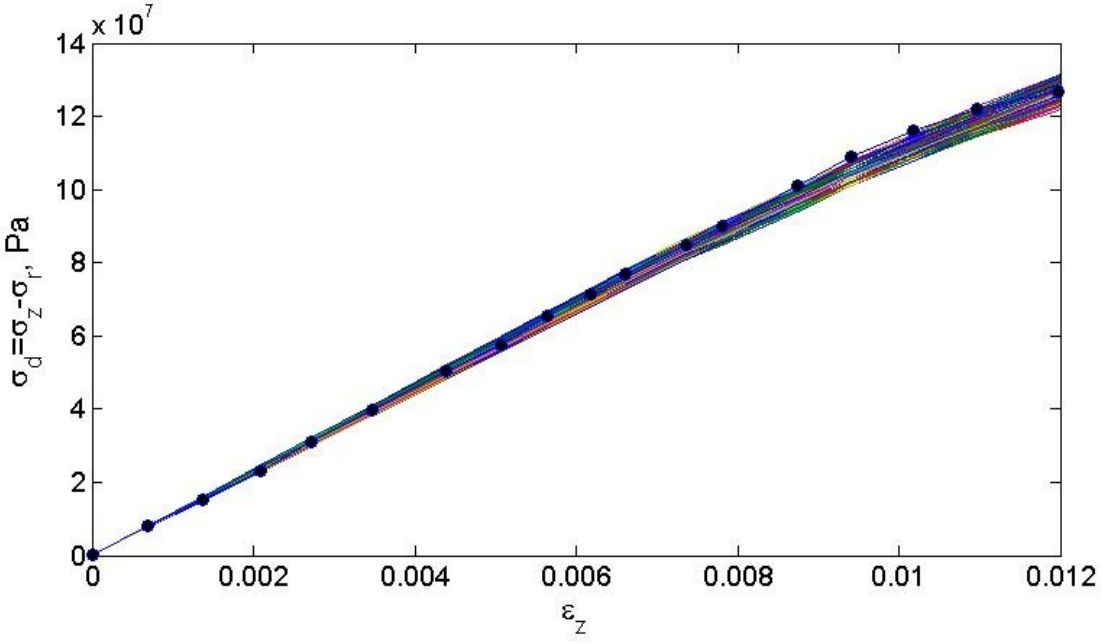
x 10^7
14
12
10
8
6
4
2
0
0
0.002
0.004
0.006
0.008
0.01
0.012
σd=σz-σr, Pa
εz

Figure 4:

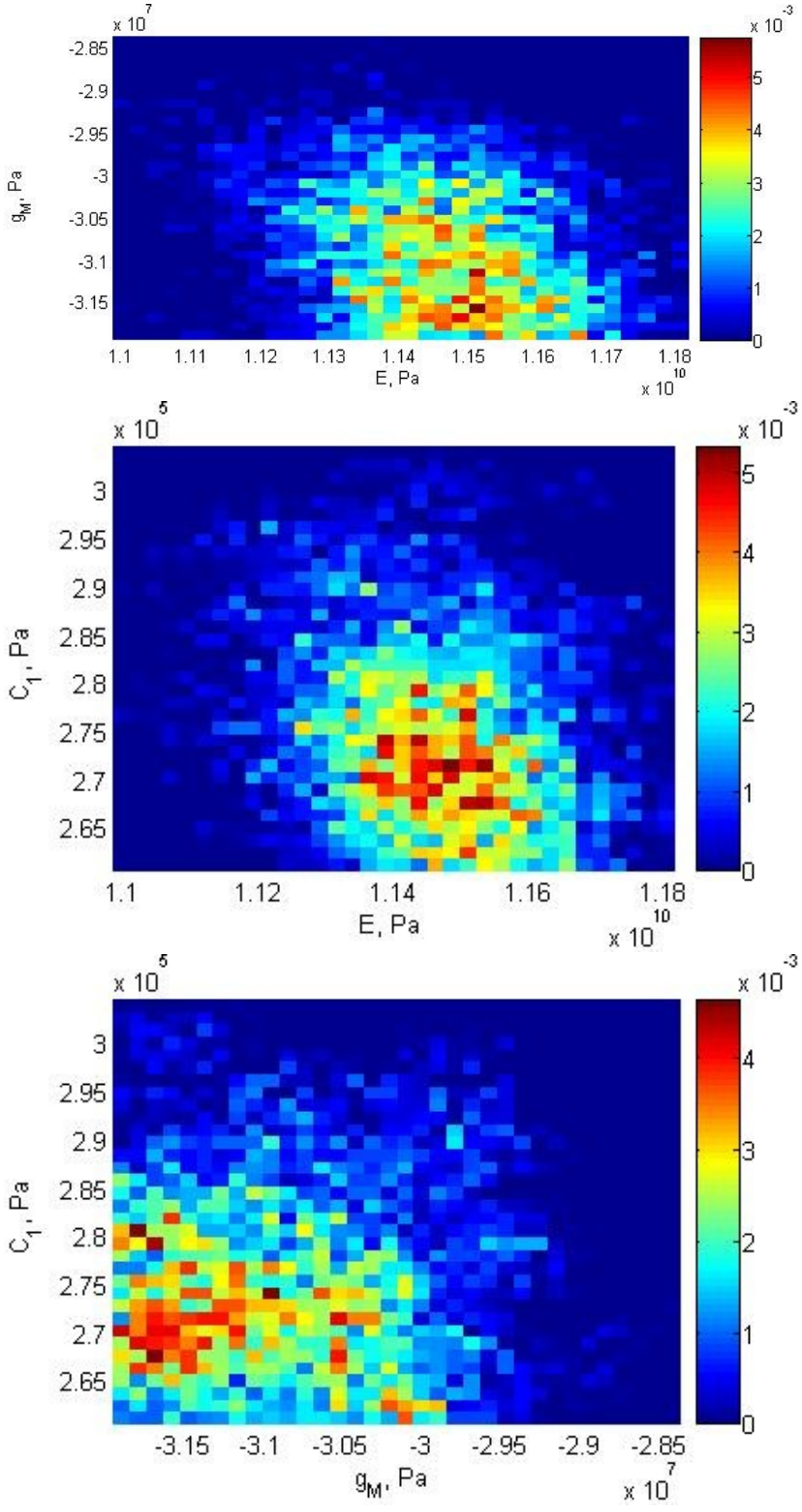
x 10^7
-2.85
-2.9
-2.95
-3
-3.05
-3.1
-3.15
g_M, Pa
1.1
1.11
1.12
1.13
1.14
1.15
1.16
1.17
1.18
E, Pa
x 10^10
x 10^-3
5
4
3
2
1
0
x 10^5
3
2.95
2.9
2.85
2.8
2.75
2.7
2.65
C_1, Pa
1.1
1.12
1.14
1.16
1.18
E, Pa
x 10^10
x 10^-3
5
4
3
2
1
0
x 10^5
3
2.95
2.9
2.85
2.8
2.75
2.7
2.65
C_1, Pa
-3.15
-3.1
-3.05
-3
-2.95
-2.9
-2.85
g_M, Pa
x 10^7
x 10^-3
4
3
2
1
0

Figure 5:

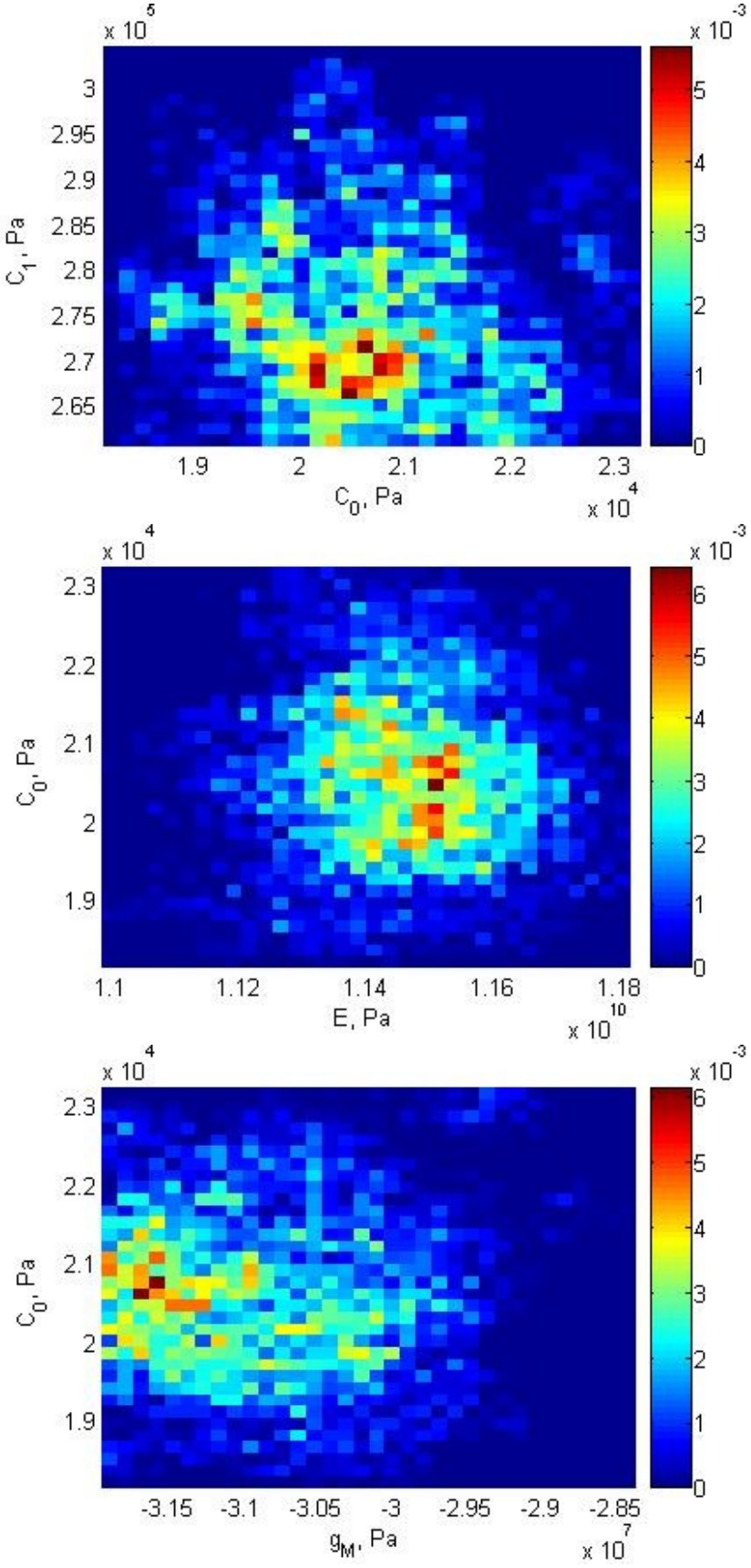
x 10^5
x 10^-3
3
2.95
2.9
2.85
2.8
2.75
2.7
2.65
C1, Pa
1.9
2
2.1
2.2
2.3
C0, Pa
x 10^4
x 10^4
x 10^-3
2.3
2.2
2.1
2
1.9
C0, Pa
1.1
1.12
1.14
1.16
1.18
E, Pa
x 10^10
x 10^4
x 10^-3
2.3
2.2
2.1
2
1.9
C0, Pa
-3.15
-3.1
-3.05
-3
-2.95
-2.9
-2.85
gM, Pa
x 10^7

Figure 6: